Local fields in conductor surface electromigration: A first-principles study in the low-bias ballistic limit

Kirk H. Bevan, Wenguang Zhu, G. Malcolm Stocks, Hong Guo, and Zhenyu Zhang

Phys. Rev. B **85**, 235421 — Published 8 June 2012

DOI: 10.1103/PhysRevB.85.235421

Local fields in conductor surface electromigration: a first-principles study in the low bias ballistic limit

Kirk H. Bevan*,[1,2] Wenguang Zhu,[3,2] G. Malcolm Stocks,[2] Hong Guo,[4] and Zhenyu Zhang[5,6]

[1]*Department of Mining and Materials Engineering, McGill University, Montreal, QC H3A 0C5, Canada*
[2]*Materials Science and Technology Division, Oak Ridge National Laboratory, Oak Ridge, TN 37831, USA*
[3]*Department of Physics and Astronomy, University of Tennessee, Knoxville, Tennessee 37996, USA*
[4]*Centre for the Physics of Materials and Department of Physics, McGill University, Montreal, QC H3A 2T8, Canada*
[5]*Department of Physics and Astronomy, University of Tennessee, Knoxville, TN 37996, USA*
[6]*ICQD, University of Science and Technology of China, Hefei, Anhui 230026, China*

Utilizing first-principles quantum transport calculations, we investigate the role of local fields in conductor surface electromigration. A nanometer thick Ag(100) thin film is adopted as our prototypical conductor, where we demonstrate the existence of intense local electric fields at atomic surface defects under an external bias. It is shown that such local fields can play an important role in driving surface electromigration and electrical breakdown. The intense fields originate from the relatively short (atomic-scale) screening lengths common to most elemental metals. This general short-range screening trend is established self-consistently within an intuitive picture of linear response electrostatics. The findings shed new light on the underlying physical origins of surface electromigration and point to the possibility of harnessing local fields to engineer electromigration at the nanoscale.

PACS numbers: 71.15.-m,73.22.-f,73.40.-c,73.63.-b

I. INTRODUCTION

Over the past decade semiconductor device dimensions have rapidly approached the 10 nm nanoelectronic milestone.[1,2] In tandem to this effort, there has been a corresponding size reduction in the metallic wires (or interconnects) which tie nanoelectronic devices together to form logic circuits.[3] At such small dimensions, surfaces heavily influence the physical properties of conductors.[4–6] In particular, surface electromigration (EM)[7,8] often leads to the rapid breakdown of nanoscale conductors,[4,9] and is therefore a major reliability and performance concern in modern computer chip design.[3,9,10] For this reason, EM continues to attract a great deal of applied and fundamental research interest in physics,[4,11] chemistry,[5,11–13] materials science,[9,14] and nanoelectronics.[4,9–11,14,15] The impetus to further our understanding of EM, arises from a desire to realize full control over EM at both the fundamental level of chemical bond breaking[5,11–13,16] but also within the grander scope of nanoscale materials design.[4,5,9,11,12,14,15,17] Within the context of these practical and pressing surface EM concerns, this paper delves into the fundamental origins of EM at the nanoscale.

Conventionally, conductor EM is understood semiclassically in terms of a driving wind force.[18–21] When a bias is applied across a conductor, charge carriers scatter against atomic defects such as surface step edges or adatoms[4,7,22] as shown in Fig. 1. Following the principle of momentum conservation as dictated by Newton's laws: electron momentum lost through elastic scattering is transferred at a rate determined by the current density, such that electron momentum transferred over time acts as an "electron wind" that pushes defect atoms along.[4,19,21,23] Beyond this semiclassical perspective there is, however, a second important and often overlooked driving force in EM that is contributed by the voltage drop ϕ_d near an electromigrating atom as shown in Fig. 1.[19,21,24] Though it is generally assumed to be much weaker than the wind force, various models disagree on the role of the voltage drop in EM and the precise magnitude of the electric field $\vec{\nabla}\phi_d$ at an electromigrating atom.[18,19,21,23–28] In particular, the extent to which the electric field is screened from electromigrating atoms, and the role of external field inhomogeneities near an electromigrating atom both remain unresolved.[18,19,21,29,30] These questions remain unresolved, to a large extent, because the conventional separation of the EM force into electric field and electron-wind components is somewhat artificial.[24] Meaning, local fields and currents are manifestations of the same *non-equilibrium* charge density and are therefore not readily decoupled as we demonstrate herein.[21]

Building upon our recent work (Ref. 18), where EM was examined without considering the role of the voltage drop, in this work we now consider the role of the voltage drop in EM at low biases (where EM commonly occurs).[4,21,28] We show rather surprisingly, though first-principles quantum transport calculations,[18,31] that EM at the surfaces of nanoscale conductors is often determined by the local external field[28] rather than the wind force.[18,19,21,23–25,27] When conductor dimensions approach the nanoscale, surface defects do not merely contribute to EM but also increasingly contribute to resistivity (via surface roughness scattering).[3,6,32] In the elastic scattering limit, surface resistivity induces a

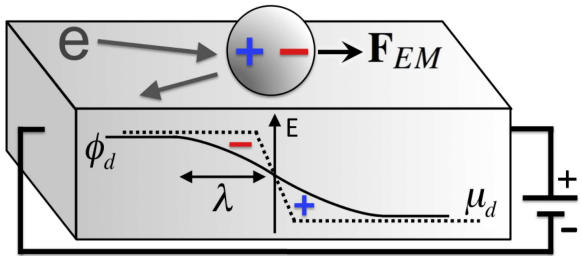

FIG. 1: (Color online) Electromigrating atom experiencing a force $\mathbf{F}_{EM}$ at the surface of a nanoscale conductor subject to an applied bias (shown as a battery). Conventional viewpoint: (surface) carriers elastically scatter off a defect and transfer momentum giving rise to a wind force. Viewpoint we present here: (interior of atom and conductor) the voltage drop ϕ_d (solid line) imparts an EM force and follows the electrochemical drop μ_d (dotted line) at a scatterer after a screening length λ. This force is equal and opposite to that imparted on the atom by the non-equilibrium screening charge $\delta\rho_e$. Accumulation and depletion of $\delta\rho_e$, in red and blue respectively, arises where the electrostatic potential ϕ_d does not follow the electrochemical potential μ_d.

strong localization of the voltage drop near electromigrating atoms.[22,33] Due to this correlation, strong external field inhomogeneities are shown to often arise *within* a screening length surrounding an atomic defect (as illustrated in Fig. 1) and act to drive EM. Moreover, we show that the voltage drop contribution to EM can be understood through linear response electrostatics[25,34–36] as a broad phenomenon occurring in conductors with screening lengths approaching one bond length. This criteria is met by most elemental metals, including technologically important metals such as: Ag, Cu, Ti, Ta, Au, Pb, Al, Fe, Co, Ni, W, and Pt.[2,37] In general, the results provide a new possible route for controlling and engineering EM in nanoelectronic systems[4,5,9,11,12,14,15,33] through local applied fields.

II. METHOD

Our model EM conductor is an ultra-thin silver film 6 atomic layers thick.[4,38,39] Specifically, we chose nanometer thick Ag(100)[38] with adatom chain and step edge surface defects[4,7,10,40] as displayed in Fig. 2a. Recent breakthroughs in quantifying EM at the nanoscale have been achieved atop Ag thin films[4,22] – where step edge defects were shown to be the primary source of conductor EM.[4] Furthermore, the intriguing phenomena of quantum growth allows the fabrication of Ag thin films with thicknesses down to several atomic layers.[38,39]

Both geometries presented in Fig. 2a were relaxed within the VASP software package,[41] where electron-ion interactions are represented through the projector augmented wave (PAW) method.[42,43] Each geometry was periodically repeated to form slabs separated a vacuum region of 12 Å. Electron exchange-correlation interactions were captured within the generalized gradient approximation (PBE-GGA).[44] The default VASP-PAW potential database Ag plane-wave cutoff energy of 249.846 eV was applied. To aid convergence, the Fermi-level smearing approach of Methfessel and Paxton[45] was employed at a Gaussian width of 0.1 eV. Optimized atomic geometries were achieved when forces on all unconstrained atoms were smaller in magnitude than 0.01 eV/Å. The Ag bulk 4.17 Å lattice constant obtained by this approach matched reasonably well with the experimental value of 4.09 Å.[46] The general conclusions of our study are unchanged by such small variations in the assumed Ag lattice constant.

After relaxing the atomic structures, EM and transport properties were calculated by carrying out DFT within the Keldysh non-equilibrium Green's functions (NEGF) formalism.[18,31] A linear combination of atomic orbitals (LCAO) were used to describe valence electrons and norm-conserving pseudopotentials were used to approximate atomic cores.[47,48] To insure a proper work function, a double-ζ polarized basis set confined at 0.0025 Ry was adopted. The 4d-electrons were included. An Ag partial core density was included to accurately capture exchange-correlation interactions near the core region.[48–50] Exchange-correlation interactions were captured through the local density approximation (LDA) on a real space grid of 4 points per Bohr. To guarantee accurate representation of the Fermi surface, the Brillouin zone transverse to the direction of transport was sampled at 256 k_x-points (see Fig. 2a). The total device region simulated was 3.5 nm in length. The applied voltage drop and its field gradient were computed self-consistently within NEGF-DFT (for further details see Refs. 31 and 51). Lastly, due to the small bias voltages considered, self-consistent calculations were judged to have converged when every element of the density matrix was converged to less than 10^{-8} a.u. at a Green's function integral resolution of 136 energy points.[31,51] Such transport calculations were found to be very computationally time consuming, amounting to approximately 45,000 computing core hours. Extensive details on the EM force computation approach, applied to the above transport calculations, can be found in the appendix to this paper.

III. RESULTS & DISCUSSION

Upon applying a bias of $\mu_L - \mu_R$, a net increase in left scattering electrons (red) and decrease in right scattering electrons (blue) impacts upon a defect,[18,52] as shown diagrammatically in Fig. 2b and explicitly through atomistic NEGF-DFT calculations in Fig. 3a for chain and step defects. In nanoscale conductors with dimensions approaching 10nm, conductivity is determined by many such surface scattering events.[3,6,32] In this regime, where elastic scattering dominates, the cumulative voltage drop across many defects can be approximated as a series of

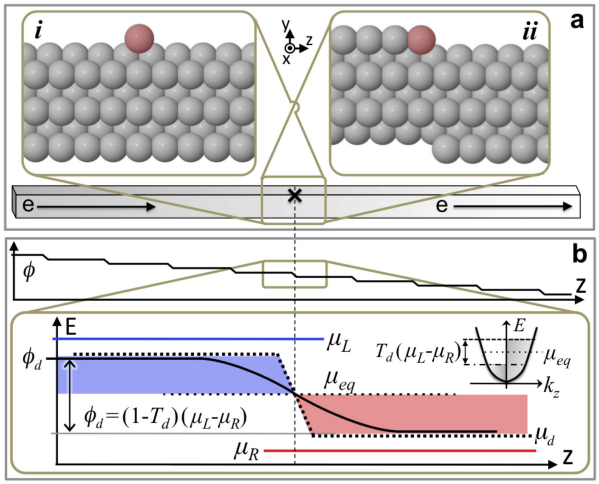

FIG. 2: (Color online) (a) Model system consists of an Ag(100) 1nm thin film. Magnification displays the Ag atoms (red) for which we compute EM forces: (a,i) adatom chain; and (a,ii) step edge. (b) In the elastic scattering limit the voltage, ϕ, drops discretely at each defect. Magnification provides an energetic representation: an applied bias of $\mu_L - \mu_R$ induces an increase in right scattering electrons (blue) and a decrease in left scattering electrons (red); the degree to which the electrostatic potential drop ϕ_d at a defect follows the applied bias $\mu_L - \mu_R$ is determined by the electron transmission T_d.[34]

discrete events (ϕ_d) occurring within a screening length of each defect as shown diagrammatically in Fig. 2b.[33] Within NEGF-DFT, the voltage drop due to an atomic sized scatterer can be calculated explicitly[31,51] as shown for the model chain and step defects in Fig. 3b.

Phenomenologically, the voltage drop at each defect can be correlated to the electrochemical potential bias between the left scattering (μ_L) and right scattering (μ_R) electrons (see Fig. 2b) through the average probability of electron transmission $0 \leq T_d \leq 1$ via $\phi_d = (1 - T_d)(\mu_L - \mu_R)$;[34] such that a sizable current with an energy window width of $T_d(\mu_L - \mu_R)$ is carried past each defect, leading to the conductor averaged shifted Fermi sphere *energy v.s. momentum* (E *v.s.* k_z) distribution shown in Fig. 2b.

The *non-equilibrium* EM force that arises upon applying a bias, is imparted by the *external field* voltage drop ϕ_d which arises from the non-equilibrium screening charge density $\delta\rho_e$ as shown in Fig. 1.[18,21,28] How one defines the relationship between the voltage drop ϕ_d and the non-equilibrium charge density $\delta\rho_e$, fundamentally determines how EM forces are calculated.[18,19,21,23–25,27] When including the voltage drop ϕ_d self-consistently within density functional theory (DFT), following the Feynman-Hellmann theorem,[18,24] at low bias the total EM force ($\mathbf{F}_{EM}$) on a defect within is expressed as[18,24]

$$\begin{aligned}\mathbf{F}_{EM} &= -\int \left(\rho_{e,j}\vec{\nabla}\phi_d + \rho_{c,j}\vec{\nabla}\phi_d^H\right) d\mathbf{r} \\ &= -\int \frac{\partial V}{\partial \mathbf{R}_j}\delta\rho_e d\mathbf{r}, \end{aligned} \quad (1)$$

where $\mathbf{R}_j$ defines the defect atom position and V is the crystal potential (see the appendix to this paper). The defect is assigned the index of the j^{th} atom in the system. The first term in Eq. (1) describes the electrostatic force exerted by the external field $\vec{\nabla}\phi_d$ upon both the defect electron charge density $\rho_{e,j}$ and core nuclear charge density $\rho_{c,j}$.[53–55] Within DFT, as applied herein, the exchange-correlation (XC) contribution to $\phi_d = \phi_d^{XC} + \phi_d^H$ acts only on the defect electron density $\rho_{e,j}$; whereas, the Hartree contribution ϕ_d^H acts on both $\rho_{e,j}$ and $\rho_{c,j}$ (see the appendix). The second term in Eq. (1) describes the electrostatic force $-\partial V/\partial \mathbf{R}_j$ exerted on the screening charge density $\delta\rho_e$ by the electromigrating atom.[24] *Meaning, the force exerted on the electromigrating atom by the external field* $\vec{\nabla}\phi_d$ *is equal and opposite to the force exerted by the atom on the external charge density* $\delta\rho_e$ *which produces* ϕ_d. This follows from Coulomb's law through Newton's third law. Herein, we demonstrate that the voltage drop ϕ_d in Eq. (1) can be correlated to the sharp electrochemical potential drop μ_d at a defect imparted by an external source, such as an electrochemical battery, through the conductor screening length λ (as shown in Fig. 1).[34] In most elemental metals the screening length λ is on the order of one bond length,[37] such that the electrostatic potential ϕ_d closely follows the electrochemical potential μ_d. This leads to strong local fields $\vec{\nabla}\phi_d$ which drive EM as we show for our model Ag system.

On the other hand, the wind force approximation sidesteps the self-consistent ϕ_d field present in Eq. (1), by assuming that the EM force acting on a defect is primarily imparted by electrons scattering elastically within the bias window $\mu_L - \mu_R$ as shown in Fig. 2b (see also Fig. 1). Hence, the EM force is usually approximated as a wind force $\mathbf{F}_W$[18,19,21,24,56]

$$\mathbf{F}_{EM} \approx \mathbf{F}_W = -\int \frac{\partial V}{\partial \mathbf{R}_j}\delta\rho_e^s d\mathbf{r}, \quad (2)$$

where $\delta\rho_e^s = (\mu_L - \mu_R)[\rho_L(\mu_{eq}) - \rho_R(\mu_{eq})]/2$ and $\rho_{L,R}(\mu_{eq})$ is the left/right scattering electron density at the equilibrium electrochemical potential μ_{eq}. This amounts to dropping the self-consistent contributions in Eq. (1), and approximating the non-equilibrium charge density by the bias window scattering charge density $\delta\rho_e \approx \delta\rho_e^s$ displayed in Fig. 3a (for further details see the appendix). At the nanoscale, the wind force approximation (summarized by Eq. (2)) is only strictly valid in materials possessing a low Fermi electron density $\rho(\mu_{eq}) = \rho_L(\mu_{eq}) + \rho_R(\mu_{eq})$. Most elemental metals possess a short screening length comparable to that of

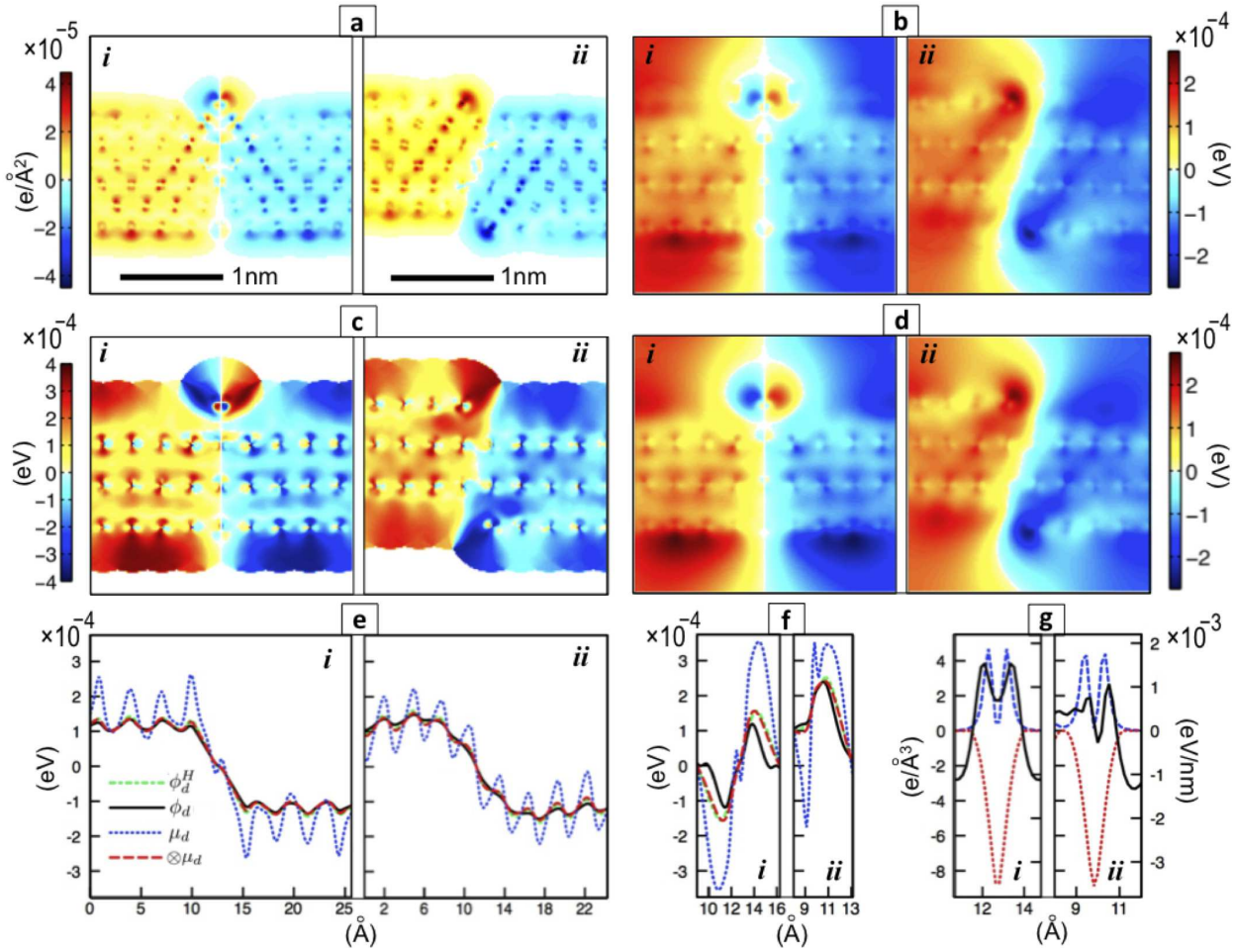

FIG. 3: (Color online) EM forces acting on chain (i) and step edge (ii) defects atop an Ag(100) 1nm thin film in the elastic scattering limit. (a) The bias window electron scattering charge density $\int \delta\rho_e^s dx = \int(\mu_L - \mu_R)[\rho_L(\mu_{eq},\mathbf{r}) - \rho_R(\mu_{eq},\mathbf{r})]dx/2$, nanometer bar shows the length scale of plots (a) through (d). (b) The self-consistent voltage drop $\phi_d(\mathbf{r})$ arising from an applied $\mu_L - \mu_R = 1$ meV bias. (c) The local electrochemical potential $\mu_d(\mathbf{r})$ perturbation via Eq. (5). (d) The linear response Hartree solution to ϕ_d^H via Eq. (6). (e) The voltage drop in the center of the film (solid black). (f) The voltage drop inside the each defect (solid black). In (e) and (f) the self-consistent Hartree potential (dot-dashed green), electrochemical potential (dotted blue), and convolved electrochemical potential (dashed red) are also given – where the convolution symbol $\otimes$ denotes the solution arrived at via Eq. (6). In (g) the electric field (solid black, right axis) inside each defect plotted against the valence electron (dashed blue, left axis) and pseudo-core charge[48] (dotted red, left axis) densities.

Ag,[37] and in such short screening metals nanoscale EM is often driven by the voltage drop ϕ_d in Eq. (1) as we show below.[57]

When a bias is applied, the voltage drop ϕ_d at a defect (as calculated for our model Ag system in Fig. 3b) is arrived at self-consistently within NEGF-DFT by solving Poisson's equation[21,28,31,35,51]

$$\nabla^2 \phi_d^H(\mathbf{r}) = -\frac{e\delta\rho_e}{\varepsilon}, \tag{3}$$

which relates the Hartree contribution ϕ_d^H within the voltage drop ϕ_d to the non-equilibrium screening charge density $\delta\rho_e$ (e, electron charge; $\varepsilon = \varepsilon_0$, permittivity of free space). Further minor exchange-correlation terms are included in the total non-equilibrium self-consistent perturbation $\phi_d = \phi_d^H + \phi_d^{XC}$ presented in Fig. 3b. At the low local biases required to drive EM in conductors,[18,22] the non-equilibrium charge $\delta\rho_e$ is determined by the degree to which the electrostatic potential ϕ_d^H does not follow the electrochemical potential μ_d,[34] such that

$$\delta\rho_e(\mathbf{r}) \approx \rho(\mu_{eq},\mathbf{r})[\mu_d(\mathbf{r}) - \phi_d^H(\mathbf{r})] \tag{4}$$

where $\rho(\mu_{eq}) = \rho_L(\mu_{eq}) + \rho_R(\mu_{eq})$ is the local density of states at the Fermi energy (μ_{eq}). In the linear-response regime considered here, the local perturbation to the electrochemical potential is defined as[25,34]

$$\mu_d(\mathbf{r}) = \frac{\mu_L - \mu_R}{2}\left[\frac{\rho_L(\mu_{eq},\mathbf{r}) - \rho_R(\mu_{eq},\mathbf{r})}{\rho_L(\mu_{eq},\mathbf{r}) + \rho_R(\mu_{eq},\mathbf{r})}\right], \tag{5}$$

and is plotted in Fig. 3c for the model chain and step defects – where it can be seen that the electrochemical potential follows the non-equilibrium scattering electron density in Fig. 3a. By rearranging terms in Eq. (3) after inserting Eq. (4), we arrive at a linear-response or low bias formulation of Poisson's equation[34,35,58,59]

$$[\nabla^2 - \frac{e\rho(\mu_{eq},\mathbf{r})}{\varepsilon}]\phi_d^H(\mathbf{r}) = -\frac{e\rho(\mu_{eq},\mathbf{r})}{\varepsilon}\mu_d(\mathbf{r}). \quad (6)$$

Upon plugging in $\mu_d(\mathbf{r})$ and $\rho(\mu_{eq},\mathbf{r})$, Eq. (6) yields the linear-response Hartree solutions displayed in Fig. 3d. It can be seen that the self-consistent solutions in Fig. 3b and linear-response Poisson solutions in Fig. 3d are nearly identical, with minor differences arising (for both chain and step defects) due to the exchange-correlation potential correction ϕ_d^{XC}. This agreement is further solidified in Fig. 3e and Fig. 3f, where the Hartree term of the self-consistent solution (in dot dashed green) follows the linear-response Hartree solution (in dashed red). In essence, the electrostatic potential $\phi_d^H(\mathbf{r})$ is a smoothening convolution of the electrochemical potential $\mu_d(\mathbf{r})$ dictated by the screening length of Ag ($\lambda = \sqrt{\varepsilon/e\rho(\mu_{eq})} \rightarrow \lambda_{Ag} \approx 2.5$Å, as shown in Fig. 3e).[28,34,35] In most elemental metals such as Ag, Cu, Ti, Ta, Au, Pb, Al, Fe, Co, Ni, W, and Pt, the density of states at the Fermi energy is very high and the screening length is therefore very short (close to one bond length).[37,60,61]

The above correlation between the electrostatic potential ϕ_d and electrochemical potential μ_d, contains a subtle and yet important insight into the theoretical treatment of EM at the nanoscale. Specifically, from Eq. (3) through to Eq. (6) we can see that the wind force approximation is only valid in conductors where the screening length ($\lambda = \sqrt{\varepsilon/e\rho(\mu_{eq})}$) is sufficiently long (on an atomistic scale) such that the voltage drop at a defect can be ignored. Since, applying the wind force approximation central assumption (that the non-equilibrium electron density $\delta\rho_e$ within an electromigrating atom is well approximated by the bias window scattering charge density $\delta\rho_e \approx \delta\rho_e^s$) to Eq. (4) yields $\phi_d^H = 0$. In conductors where the screening length is several nanometers or more, for example heavily doped semiconductors,[34] it is probably reasonable to assume that the voltage drop is negligible ($\phi_d^H \approx 0$) at an atomic defect.[18,28,34,35] *However, in conductors such as Ag possessing very high conducting electron densities, or high conductivity, and screening lengths measured in angstroms ($\lambda_{Ag} \approx 2.5$Å): local perturbations to the electrochemical potential $\mu_d(\mathbf{r})$ by non-equilibrium scattering electrons are not smoothened by the screening length (λ) to such an extent that the voltage drop $\phi_d(\mathbf{r})$ at a defect can be safely ignored.* This short screening length phenomena is clearly demonstrated in Fig. 3f, where we see that the local electrochemical potential perturbation (μ_d in dotted blue) gives rise to significant self-consistent external fields (ϕ_d in black) within the model Ag(100) chain and step defects.

The precise role of local fields in conductor EM can be determined by directly applying Eq. (1) to the self-consistent results in Fig. 3. For the Ag(100) chain defect and step defects displayed in Fig. 2a, the self-consistent EM forces were calculated to be $\mathbf{F}_{EM,i} = 2.1 \times 10^{-3}\hat{\mathbf{z}}$ eV/nm and $\mathbf{F}_{EM,ii} = 2.0 \times 10^{-4}\hat{\mathbf{y}} + 9.9 \times 10^{-4}\hat{\mathbf{z}}$ eV/nm at a bias of 1meV.[18,55] The force magnitude $|\mathbf{F}_{EM}|$ is plotted in Fig. 4 (x's), where it can be seen that the force exerted on each defect by the external field ϕ_d (black x's) is equal to the force exerted by the defect on the external charge $\delta\rho_e$ (red x's). This follows from Coulomb's law through Newton's third law. On the other hand, as discussed earlier, the wind force force approximation $|\mathbf{F}_W|$ (blue squares) expressed by Eq. (2) can be seen to grossly overestimate the Ag EM force magnitude (having said that, the force direction agrees well).[18,62]

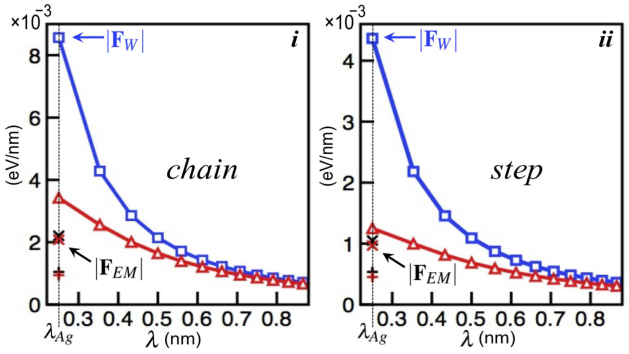

FIG. 4: (Color online) EM force magnitude as a function of the screening length: (i) chain and (ii) step. External field linear response solution to Eq. (1) shown in red triangles. Wind force solution to Eq. (2) in blue squares. Fully self-consistent solutions to Eq. (1): Hartree Coulomb force in crosses and Hartree plus exchange-correlation total EM force in x's. Force exerted by the external field ϕ_d on the defect in black and force exerted by the defect on the external charge $\delta\rho_e$ in red (for all symbol assignments).

Though $\mathbf{F}_W$ is a less than ideal approximation to $\mathbf{F}_{EM}$ in short screening metals such as Ag, we can extrapolate to longer screening lengths and determine when the wind force approximation should agree well with the self-consistent force. By solving for the linear response screening charge density in Eq. (4) at lower Fermi electron densities, simply obtained by dividing $\rho(\mu_{eq})$ by a real positive number, we can estimate estimate $|\mathbf{F}_{EM}|$ at longer screening lengths (λ). The linear response estimate to $|\mathbf{F}_{EM}|$ is shown in Fig. 4 (red triangles), where it can be seen to approach $|\mathbf{F}_W|$ (blue squares) as $\lambda \rightarrow 1$nm for both the model chain and step defects.[28] Interestingly, the self-consistent force decays inversely with the screening length ($1/\lambda$) and the wind force decays proportionally to the Fermi electron density (or with $1/\lambda^2$). Hence, in materials with screening lengths greater than or equal to 1nm the wind force approximation is likely reasonable. However, in shorter screening length materials, which includes most elemental metals, the external field should be included explicitly to arrive at physically meaningful EM force estimates.[63]

IV. CONCLUSION

In summary, we have shown, through first-principles quantum transport calculations, that local fields play an important role in nanoscale conductor EM (in the ballistic limit). We argue that this somewhat counter intuitive result, where the wind force is conventionally assumed to drive EM,[18] can be understood intuitively in terms of characteristic screening lengths. In most elemental metals, such as the model Ag(100) thin film investigated, the screening length is so short[37] that voltage fields can arise internally within electromigrating atoms to drive EM. Specifically, the results suggest the intriguing possibility of limiting nanoelectronics interconnect surface EM driven breakdown by tuning the conducting electron density near surface defects.[3,4,6,7,10,30] In general, the results present a new engineering variable, namely the local external field, for harnessing and controlling EM in novel nanoelectronic devices and architectures.[4,5,9,11,12,14,15,17,33]

ACKNOWLEDGMENTS

We thank S. Datta for helpful discussions on resistivity dipoles and E. D. Williams for discussions on fields in EM. This work was supported in part by NSERC of Canada, FRQNT of Quebec and CIFAR, US-NSF (DMR-0906025), and the Division of Materials Sciences and Engineering, Office of Basic Energy Sciences, US-DOE. Computational support was provided by the NSF Network for Computational Nanotechnology and NERSC of US-DOE.

*Electronic address: kirk.bevan@mcgill.ca

APPENDIX : ELECTROMIGRATION FORCE COMPUTATION METHODS

1. The Low Bias Electromigration Force

Within the two probe Landauer-Büttiker picture, the force contribution from scattering electrons for an atom at position $\mathbf{R}_j$ is given by[18]

$$\mathbf{F}_e = -\int \frac{\partial V}{\partial \mathbf{R}_j}[\rho_L(E)f_L(E) + \rho_R(E)f_R(E)]dEd\mathbf{r}, \tag{A1}$$

where $\rho_{L,R}(E)$ represents the left/right electron scattering density from the left/right contact at energy E.[18,34] The total system potential V includes field contributions from all atomic electrons and all nuclei. In the case of a neutral atom at position $\mathbf{R}_j$, the nuclear field is well screened outside the valence electron density.[48] The quantity $f_{L,R}(E) = 1/(1 + e^{(E-\mu_{L,R})/k_BT})$ defines the Fermi occupancy of left/right scattering electrons. At zero bias when both reservoirs posses the same temperature T and electrochemical potential ($\mu_{eq} = \mu_L = \mu_R$), there is no net electron flux and the EM force is by definition *zero*.

When a bias is applied such that $\mu_L \neq \mu_R$ as shown in Fig. 2, a net non-zero driving EM force $\mathbf{F}_{EM}$ arises from the *elastic scattering* of current carrying electrons.[21] In the low bias regime the total non-equilibrium EM force can be determined by subtracting the zero bias electronic force contribution from the biased electronic force contribution,[18,24]

$$\begin{aligned}\mathbf{F}_{EM} &= \mathbf{F}_e^{bias} - \mathbf{F}_e^{eq} \\ &= -\int \frac{\partial V}{\partial \mathbf{R}_j}[\rho_L^{bias}(E)f_L(E) + \rho_R^{bias}(E)f_R(E)]dEd\mathbf{r} \\ &+ \int \frac{\partial V}{\partial \mathbf{R}_j}[\rho_L^{eq}(E)f_{eq}(E) + \rho_R^{eq}(E)f_{eq}(E)]dEd\mathbf{r} \\ &= -\int \frac{\partial V}{\partial \mathbf{R}_j}\delta\rho_e d\mathbf{r},\end{aligned} \tag{A2}$$

which essentially describes the electrostatic force imparted by the atom at $\mathbf{R}_j$ on the non-equilibrium charge density $\delta\rho_e$. From this perspective it is very reasonable to invoke Newton's third law to obtain,

$$\begin{aligned}\mathbf{F}_{EM} &= -\int \frac{\partial V}{\partial \mathbf{R}_j}\delta\rho_e d\mathbf{r} \\ &= -\int \left(\rho_{e,j}\vec{\nabla}\phi_d + \rho_{c,j}\vec{\nabla}\phi_d^H\right) d\mathbf{r}.\end{aligned} \tag{A3}$$

By Newton's third law, through Coulomb's law, the external potential voltage drop ϕ_d produced by $\delta\rho_e$[28] acts with equal and opposite force on the electromigrating atom at position $\mathbf{R}_j$. Meaning, the non-equilibrium charge density $\delta\rho_e$ and the atom at position $\mathbf{R}_j$ act on each other with equal and opposite forces. Eq. (A3) is expressed within DFT, the non-equilibrium electron density $\delta\rho_e$ and the defect electron density $\rho_{e,j}$ interact with each other through equal and opposite Hartree (H) and exchange-correlation (XC) forces (where, $\phi_d = \phi_d^H + \phi_d^{XC}$).[64] However, $\delta\rho_e$ and the nuclear core charge $\rho_{c,j}$ only interact with each other through equal and opposite Hartree forces.

In this work, the self-consistent charge density given by $\rho_{e,j}$ corresponds to the pseudopotential valence electron density $\rho_{v,j}$ of the electromigrating atom, and is determined through Mulliken population analysis of the conducting system.[53–55] The combined frozen core electron density and nuclear charge in Eq. (A3) is approximated by $\rho_{c,j}$ (see the pseudopotential discussion pertaining to Eq. (A15) at the end of this appendix). When computing exchange-correlation interactions, the defect partial core density $\rho_{pc,j}$ is also included. Hence, within the pseudopotential approach applied[48] Eq. (A3) is approximated

as

$$\mathbf{F}_{EM} = -\int \Big[(\rho_{v,j}+\rho_{pc,j})\vec{\nabla}\phi_d^{XC} + (\rho_{v,j}+\rho_{c,j})\vec{\nabla}\phi_d^{H}\Big] d\mathbf{r}. \tag{A4}$$

In an all-electron calculation Eq. (A3) can be applied,[62] where $\rho_{e,j}$ would include all bound electrons and $\rho_{c,j}$ would correspond to the nuclear charge of the atom at $\mathbf{R}_j$. Likewise, Eq. (A2) is captured through the same pseudopotential approach (see the last section of this appendix). The screened nuclear field $\partial V/\partial \mathbf{R}_j$ acting on $\delta\rho_e$ is approximated by $\partial V/\partial \mathbf{R}_j \approx \partial(V_c + V^H[\rho_v] + V^{XC}[\rho_v + \rho_{pc}])/\partial \mathbf{R}_j$, where V contains the potential of all atoms and electrons in the system but $\partial V/\partial \mathbf{R}_j$ essentially reduces to the screened nuclear field of the j^{th} atom. Hence, the non-equilibrium electron density $\delta\rho_e$ is assumed to reside primarily outside the pseudopotential cutoff radius r_c.[62] The integrals in Eqs. (A2) and (A4) are performed on a real-space grid.[51] The screened nuclear field of an electromigrating atom is computed numerically by self-consistently displacing the atom at $\mathbf{R}_j$ by 1×10^{-3} a.u..

2. The Low Bias Wind Force Approximation

To arrive at the wind force approximation we begin by rewriting the electronic force integral in Eq. (A1) as[18]

$$\begin{aligned}\mathbf{F}_e = -\sum_{k,s}[&\langle\Psi_L|\nabla_{\mathbf{R}_j}\hat{H}_e|\Psi_L\rangle f_L(E) \\ &+ \langle\Psi_R|\nabla_{\mathbf{R}_j}\hat{H}_e|\Psi_R\rangle f_R(E)],\end{aligned} \tag{A5}$$

where $\Psi_{L,R}$ are the left/right electron wavefunctions of the Hamiltonian $\hat{H}_e$ scattering into the device from the contacts.[18] The above summation is performed over all momentum k and spin states s. The full non-equilibrium EM force expression in Eq. (A2) is then given by,[18,24]

$$\begin{aligned}\mathbf{F}_{EM} = -\sum_{k',s'}[&\langle\Psi_L^{bias}|\nabla_{\mathbf{R}_j}\hat{H}_e^{bias}|\Psi_L^{bias}\rangle f_L(E) \\ &+ \langle\Psi_R^{bias}|\nabla_{\mathbf{R}_j}\hat{H}_e^{bias}|\Psi_R^{bias}\rangle f_R(E)] \\ &+ \sum_{k,s}[\langle\Psi_L^{eq}|\nabla_{\mathbf{R}_j}\hat{H}_e^{eq}|\Psi_L^{eq}\rangle f_{eq}(E) \\ &+ \langle\Psi_R^{eq}|\nabla_{\mathbf{R}_j}\hat{H}_e^{eq}|\Psi_R^{eq}\rangle f_{eq}(E)].\end{aligned} \tag{A6}$$

Under the wind force approximation,[21] it is assumed that the voltage drop ϕ_d can be neglected in the low bias limit. Hence, $\hat{H}_e^{bias} = \hat{H}_e^{eq} + \phi_d \approx \hat{H}_e^{eq}$ and $\Psi_{L,R}^{bias} \approx \Psi_{L,R}^{eq}$, where $\Psi_{L,R}^{bias}$ are the scattering wavefunctions of $\hat{H}_e^{bias}$. The non-equilibrium EM force in Eq. (A2) therefore reduces to the wind force $\mathbf{F}_{EM} \approx \mathbf{F}_W$,

$$\begin{aligned}\mathbf{F}_W &= -\int \frac{\partial V}{\partial \mathbf{R}_j}[\rho_L^{eq}(f_L - f_{eq}) + \rho_R^{eq}(f_R - f_{eq})]dEd\mathbf{r} \\ &= -\int \frac{\partial V}{\partial \mathbf{R}_j}\delta\rho_e^s d\mathbf{r}.\end{aligned} \tag{A7}$$

At low temperatures ($T \approx 0$) or when the density of states is energetically flat about the Fermi energy (as is the case for Ag),[37] we can approximate the low bias scattering charge density by $\delta\rho_e^s = (\mu_L - \mu_R)[\rho_L(\mu_{eq}) - \rho_R(\mu_{eq})]/2$.[21,57] The integral in Eq. (A7) is computed in the same manner as Eq. (A2) in the previous section of this appendix.

3. Force Contributions From Bound and Scattering States

In the study of EM, it is important to distinguish between bound electronic states and scattering electronic states. Bound state contributions to the non-equilibrium charge density $\delta\rho_e$ arise in response to an *electrostatic potential* perturbation. Whereas, scattering state contributions to $\delta\rho_e$ arise in response to an *electrochemical potential* perturbation.[18,34] This delineation can be obtained within the NEGF-DFT[31,51] formalism via

$$\begin{aligned}\delta\rho_e &= [\delta\rho_L + \delta\rho_R] + \delta\rho_B \\ &= \int[\rho_L^{bias}f_L + \rho_R^{bias}f_R - \rho_L^{eq}f_{eq} - \rho_R^{eq}f_{eq}]dE \\ &+ \int[\rho_B^{bias}f_{eq} - \rho_B^{eq}f_{eq}]dE,\end{aligned} \tag{A8}$$

where $[\delta\rho_L + \delta\rho_R]$ and $\delta\rho_B$ are the scattering state and bound state contributions to $\delta\rho_e$, respectively. When employing a LCAO basis set, the spin degenerate scattering and bound state charge density contributions at energy E are defined as $\rho_{L,R}(E) = G\Gamma_{L,R}G^\dagger/\pi$ and $\rho_B(E) = 2\eta GSG^\dagger/\pi$. The Green's function is given by $G = [(E+i\eta)S - \hat{H}_e - \Sigma_L - \Sigma_R]^{-1}$, where η is a small positive infinitesimal and S is the overlap matrix.[31,34,51] Finally, the left and right self-energies $\Sigma_{L,R}$ are related to the contact broadenings through $\Gamma_{L,R} = i(\Sigma_{L,R} - \Sigma_{L,R}^\dagger)$.

In the conducting limit, where $\Gamma_{L,R} \gg \eta$, scattering states perturbed by the electrochemical potential bias $\mu_L \neq \mu_R$ dominate $\delta\rho_e$. This is demonstrated, for example, through the strong agreement between the convolved electrochemical potential and the self-consistent screening potential in Fig. 3 (see the discussion surrounding Eq. (6)). Generally speaking, an electromigrating atom is strongly coupled to and broadened by the delocalized Blöch states scattering from both contacts. Hence, in the conducting limit Eq. (A2) is applied to compute EM forces.

However, in an isolated system (where $\Gamma_{L,R} \to 0$) bound states cannot be neglected. For example, an Ag

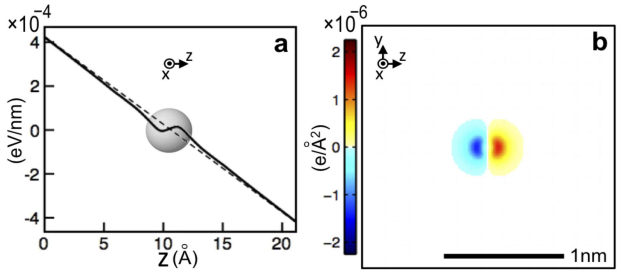

FIG. 5: (Color online) Ag atomic wire polarized by an external electric field (the wire is repeated infinitely in the $\hat{\mathbf{x}}$-direction). (a) An external field of 4×10^{-4} eV/nm (dashed line) and the external field plus the induced polarization dipole field (solid line) through the center of the wire. (b) The polarization dipole charge density $\int \delta\rho_B dx$.

atomic wire placed within a uniform electric field experiences a force due to the polarization of its bound electronic states via

$$\lim_{\Gamma_{L,R}\to 0} \mathbf{F}_{EM} = -\int \frac{\partial V}{\partial \mathbf{R}_j} \delta\rho_B d\mathbf{r}. \tag{A9}$$

Assuming an external electric field of $\sim 4 \times 10^{-4}$ eV/nm as shown in Fig. 5a, equivalent that to arising within the residual resistivity dipole of Fig. 3e, from Eq. (A9) one can arrive at a force estimate on the isolated atomic wire of $\mathbf{F}_{EM} = 1.2 \times 10^{-3}\hat{\mathbf{z}}$ eV/nm.[62] Though similar in appearance and magnitude, it is important to note that the bound state polarization in Fig. 5 is very different from the scattering state polarization in Fig. 3. The latter arises for an *electrochemical potential* perturbation of scattering states, while the former arises from an *electrostatic potential* perturbation of bound states.

4. Pseudopotential Hamiltonian Approximations

Variations of the below pseudopotential derivation can be found in several texts,[50] it is provided here for the sake of completeness (with respect to previous sections of this appendix). Within DFT, the all-electron (ae) Hamiltonian $\hat{H}^{ae}_{e,atom}$ eigenstates $|\psi_{ln}\rangle$ of an isolated atom with nuclear charge Z are given by

$$\hat{H}^{ae}_{e,atom}|\psi_{ln}\rangle = E_{ln}|\psi_{ln}\rangle$$
$$\left[-\frac{1}{2}\nabla^2 + V\right]|\psi_{ln}\rangle = E_{ln}|\psi_{ln}\rangle, \tag{A10}$$

where $V = V^H + V^{XC} - Z/r$ includes the Hartree, exchange-correlation, and nuclear potentials of the isolated atom. The indices n and l indicate the eigenstate quantum number and angular momentum, respectively. In this first part of the appendix we drop the atom index notation j since there is only one atom in this pseudopotential derivation, however we return to the index notation in the subsequent sections of this appendix. Following the norm-conserving pseudopotential conditions,[50] the all-electron valence eigenstates can be recast as

$$|\psi_{ln}\rangle = \begin{cases} |\varphi_{ln}\rangle + |\chi_{ln}\rangle & r \le r_c \\ |\varphi_{ln}\rangle & r > r_c \end{cases}, \tag{A11}$$

where $|\varphi_{ln}\rangle$ represents a valence electron pseudopotential wavefunction that is smooth in the core region and nodeless.[50] By plugging Eq. (A11) into Eq. (A10) we arrive at a non-local representation,

$$\left[\hat{H}^{ae}_{e,atom} + (\hat{H}^{ae}_{e,atom} - E_{ln})\frac{|\chi_{ln}\rangle\langle\chi_{ln}|}{\langle\chi_{ln}|\varphi_{ln}\rangle}\right]|\varphi_{ln}\rangle = E_{ln}|\varphi_{ln}\rangle. \tag{A12}$$

To exclude unphysical ghost eigenstates,[65] we approximate the screened nuclear potential acting on the valence electrons by the potential

$$\nabla^2 V_c = -4\pi\rho_c. \tag{A13}$$

The density $\rho_c(r) \propto exp[-(sinh(abr)/sinh(b))^2]$ is subject the conditions: $\rho_c(r)|_{r>r_c} = 0$, $4\pi\int|\rho_c(r)|r^2dr = Z_v$, where Z_v is the total valence electron charge.[48] In this manner the core electrons are assumed to screen the nuclear potential within $r < r_c$ such that $V_c|_{r>r_c} = -Z_v/r$. Following earlier work we have taken we have taken $b = 1$ and $a = 1.82/r_c$.[48] From Eqs. (A12) and (A13) we arrive at the smoothened non-local eigenstate equation

$$\left[-\frac{1}{2}\nabla^2 + V_c + V^H[\rho_v] + V^{XC}[\rho_v + \rho_{pc}] + \frac{|\delta V\varphi_{ln}\rangle\langle\varphi_{ln}\delta V|}{\langle\varphi_{ln}|\delta V|\varphi_{ln}\rangle}\right.$$
$$\left. -(\frac{1}{2}\nabla^2 - V + E_{ln})\frac{|\chi_{ln}\rangle\langle\chi_{ln}|}{\langle\chi_{ln}|\varphi_{ln}\rangle}\right]|\varphi_{ln}\rangle = E_{ln}|\varphi_{ln}\rangle \tag{A14}$$

where $\delta V = (V - V_c - V^H[\rho_v] - V^{XC}[\rho_v + \rho_{pc}])$, ρ_v is the pseudo valence charge density, and ρ_{pc} is the pseudo partial core density.[66] Finally, to arrive at a pseudopotential Hamiltonian $\hat{H}^{ps}_{e,atom}$ we employ $|\chi^{ps}_{ln}\rangle = \delta V|\varphi_{ln}\rangle - (\nabla^2/2 - V + E_{ln})|\chi_{ln}\rangle$ for each scattering angular momentum valence eigenstate (i.e. s, p, d, and f valence orbitals where applicable). This leads to the Hermitian representation employed herein for all NEGF-DFT[31,47,48,50,51,67] calculations

$$\hat{H}^{ps}_{e,atom} = \left[-\frac{1}{2}\nabla^2 + V_c + V^H[\rho_v] + V^{XC}[\rho_v + \rho_{pc}]\right.$$
$$\left. + \sum_l \frac{|\chi^{ps}_{ln}\rangle\langle\chi^{ps}_{ln}|}{\langle\chi^{ps}_{ln}|\varphi_{ln}\rangle}\right]. \tag{A15}$$

[1] T. N. Theis and P. M. Solomon, *Science* **327**, 1600 (2010).
[2] R. F. Service, *Science* **323**, 1000 (2009).
[3] D. Josell, S. H. Brongersma and Z. Tokei, *Annu. Rev. Mater. Res.* **39**, 231 (2009).
[4] C. G. Tao, W. G. Cullen, E. D. Williams, *Science* **328**, 736 (2010).
[5] T. Taychatanapat, K. I. Bolotin, F. Kuemmeth and D. C. Ralph, *Nano Lett.* **7**, 652 (2007).
[6] S. M. Rossnagel and T. S. Kuan, *J. Vac. Sci. Technol. B* **22**, 1071 (2004).
[7] K. H. Bevan, W. Zhu, H. Guo and Z. Zhang, *Phys. Rev. Lett.* **106**, 156404 (2011).
[8] Z. Z. Chen, N. Kioussis, K.-N. Tu, N. Ghoniem and J.-M. Yang, *Phys. Rev. Lett.* **105**, 015703 (2010).
[9] K.-C. Chen, W.-W. Wu, C.-N. Liao, L.-J. Chen and K.-N. Tu, *Science* **321**, 1066 (2008).
[10] K.-N. Tu, *J. Appl. Phys.* **94**, 545 (2003).
[11] D. B. Strukov, G. S. Snider, D. R. Stewart and R. S. Williams, *Nature* **453**, 80 (2008).
[12] G. E. Begtrup, W. Gannett, T. D. Yuzvinsky, V. H. Crespi and A. Zettl, *Nano Lett.* **9**, 1835 (2009).
[13] T. D. Yuzvinsky, W. Mickelson, S. Aloni, G. E. Begtrup, A. Kis and A. Zettl, *Nano Lett.* **6**, 2718 (2006).
[14] F. Xiong, A. D. Liao, D. Estrada and E. Pop, *Science* **332**, 568 (2011).
[15] X. Jia, M. Hofmann, V. Meunier, B. G. Sumpter, J. Campos-Delgado, J. M. Romo-Herrera, H. Son, Y.-P. Hsieh, A. Reina, J. Kong, M. Terrones and M. S. Dresselhaus, *Science* **323**, 1701 (2009).
[16] D. M. Eigler, C. P. Lutz and W. E. Rudge, *Nature* **352**, 600 (1991).
[17] S. Assefa, F. Xia and Y. A. Vlasov, *Nature* **464**, 80 (2010).
[18] K. H. Bevan, H. Guo, E. D. Williams and Z. Zhang, *Phys. Rev. B* **81**, 235416 (2010).
[19] A. H. Verbruggen, *IBM J. Res. Dev.* **32**, 93 (1988).
[20] K. H. Bevan, *MRS Proceedings* **1423**, mrsf11-1423-rr09-06 (2012).
[21] R. S. Sorbello, *Superlattice. and Microst.* **23**, 713 (1998).
[22] O. Bondarchuk, W. G. Cullen, M. Degawa, E. D. Williams, T. Bole and P. J. Rous, *Phys. Rev. Lett.* **99**, 206801 (2007).
[23] S. Heinze, N.-P. Wang and J. Tersoff, *Phys. Rev. Lett.* **95**, 186802 (2005).
[24] P. Kumar and R. S. Sorbello, *Thin Solid Films* **25**, 25 (1975).
[25] R. S. Sorbello, *Phys. Rev. B* **39**, 4984 (1989).
[26] A. Lodder, *Defect and Diffus. Forum* **77**, 77 (2007).
[27] D. Kandel and E. Kaxiras, *Phys. Rev. Lett.* **76**, 1114 (1996).
[28] G. C. Liang, A. W. Ghosh, M. Paulsson and S. Datta, *Phys. Rev. B* **69**, 115302 (2004).
[29] A. Umeno and K. Hirakawa *Appl. Phys. Lett.* **94**, 162103 (2009).
[30] R. Yongsunthon, C.-G. Tao, P. Rous and E. D. Williams, *Nanophenomena at Surfaces, Springer Series in Surface Sciences* **47**, 113 (2011).
[31] D. Waldron, L. Liu and H. Guo, *Nanotechnology* **18**, 424026 (2007).
[32] Y. Q. Ke, F. Zahid, V. Timoshevskii, K. Xia, D. Gall, and H. Guo, *Phys. Rev. B* **79**, 155406 (2009).
[33] J. Homoth, M. Wenderoth, T. Druga, L. Winking, R. G. Ulbrich, C. A. Bobisch, B. Weyers, A. Bannani, E. Zubkov, A. M. Bernhart, M. R. Kaspers and R. Moeller, *Nano Lett.* **9**, 1588 (2009).
[34] S. Datta, *Electronic Transport in Mesoscopic Systems* (Cambridge University Press, Cambridge, 1996).
[35] M. J. McLennan, Y. Lee and S. Datta, *Phys. Rev. B* **43**, 13846 (1991).
[36] S. Datta, W. D. Tian, S. H. Hong, R. Reifenberger, J. I. Henderson and C. P. Kubiak, *Phys. Rev. Lett.* **79**, 2530 (1997).
[37] D. A. Papaconstantopoulos, *Handbook of the band structure of elemental solids* (Springer, Berlin, 2011).
[38] T.-C. Chiang, *Bulletin of AAPPS* **18**, 2 (2008).
[39] Z. Y. Zhang, Q. Niu and C. K. Shih, *Phys. Rev. Lett* **80**, 5381 (1998).
[40] N. N. Negulyaev, V. S. Stepanyuk, L. Niebergall, P. Bruno, W. Hergert, J. Repp, K.-H. Rieder and G. Meyer, *Phys. Rev. Lett.* **101**, 226601 (2008).
[41] G. Kresse and J. Furthmüller, *Phys. Rev. B* **54**, 11169 (1996).
[42] P. E. Blöchl, *Phys. Rev. B* **50**, 17953 (1994).
[43] G. Kresse and D. Joubert, *Phys. Rev. B* **59**, 1758 (1999).
[44] J. P. Perdew, K. Burke and M. Ernzerhof, *Phys. Rev. Lett.* **77**, 3865 (1996).
[45] M. Methfessel and A. T. Paxton, *Phys. Rev. B* **40**, 3616 (1989).
[46] Y. Mo, W. Zhu, E. Kaxiras and Z. Zhang, *Phys. Rev. Lett.* **101**, 216101 (2008).
[47] N. Troullier and J. L. Martins, *Phys. Rev. B* **43**, 1993 (1991).
[48] J. M. Soler, E. Artacho, J. D. Gale, A. García, J. Junquera, P. Ordejón and D. Sánchez-Portal, *J. Phys.: Cond. Matt.* **14**, 2745 (2002).
[49] S. García-Gil, A. García, N. Lorente and P. Ordejón, *Phys. Rev. B* **79**, 075441 (2009).
[50] R. M. Martin, *Electronic Structure: Basic Theory and Practical Methods* (Cambridge University Press, Cambridge, 2005).
[51] J. Taylor, H. Guo and J. Wang, *Phys. Rev. B* **63**, 245407 (2001).
[52] R. Landauer, *Phys. Rev. B* **14**, 1474 (1976).
[53] The defect electron charge density $\rho_{e,j}$ can be determined through either Bader or Mulliken charge analysis.
[54] R. F. W. Bader, *Chem. Rev.* **91**, 893 (1991).
[55] R. S. Mulliken, *J. Chem. Phys.* **23**, 1833 (1955).
[56] D. N. Bly and P. J. Rous, *Phys. Rev. B* **53**, 13909 (1996).
[57] For the model Ag(100) thin film considered here, similar to all excellent conductors, only a very small bias per defect ($\mu_L - \mu_R \leq 1$ meV) is required to drive the significant current densities required for EM.[18,22] At such small biases the non-equilibrium scattering electron density is in the linear response regime, such that $\delta\rho_e^s \approx (\mu_L - \mu_R)[\rho_L(\mu_{eq}) - \rho_R(\mu_{eq})]/2$. This is particularly true for Ag, where the density of states is energetically flat around the Fermi energy (when averaged over all states in k-space).[37] The same linear response scaling applies to the voltage drop.
[58] M. Büttiker, *J. Phys.: Condens. Matter* **5**, 9361 (1993).
[59] X. Zhao, J. Wang and H. Guo, *Phys. Rev. B* **60**, 16730 (1999).
[60] W. Zhu, H. Chen, K. H. Bevan and Z. Zhang, *ACS Nano.* **5**, 3707 (2011).

[61] Generally, the screening length λ of a conductor is inversely proportional to the square root of the density of states at the Fermi energy $\rho(\mu_{eq})$ such that $\lambda = \sqrt{\varepsilon/e\rho(\mu_{eq})}$.[34] Hence, the physical meaning of Eq. (6) may be understood by assuming a spatially uniform density of states at the Fermi energy, such that the impulse response $[\nabla^2 - 1/\lambda^2]\phi_d^H = -Q\delta(\mathbf{r})/\varepsilon_o$ to a point charge Q produces the familiar Yukawa screening potential $\phi_d^H = e^{-r/\lambda}/4\pi\varepsilon_o r$.[34]

[62] All-electron NEGF calculations, more accurate than the pseudopotential approximations applied here, may be needed to fully resolve low bias EM forces. Regardless of the atomistic approximations applied, the non-equilibrium screening concepts presented here will remain essential to understanding nanoscale EM.

[63] We emphasize that this bulk density of states screening argument may not explicitly hold for every system and material. Thus, first-principles calculations of the local density of states and scattering states should be performed to determine the local screening properties of the scattering system before employing the wind force approximation (for further discussion see the appendix).[18]

[64] J. Kohanoff and N. I. Gidopoulos, *Handbook of Molecular Physics and Quantum Chemistry* (John Wiley & Sons, Chichester, 2003).

[65] X. Gonze, P. Käckell and M. Scheffler, *Phys. Rev. B* **41**, 12264 (1990).

[66] S. G. Louie, S. Froyen and M. L. Cohen, *Phys. Rev. B* **26**, 1738 (1982).

[67] L. Kleinman and D. M. Bylander, *Phys. Rev. Lett.* **48**, 1425 (1982).